J. Fluid Mech. (2014), *vol.* 749, *pp.* 79–98.
doi:10.1017/jfm.2014.208

Estimating the value of von Kármán's constant in turbulent pipe flow

S. C. C. Bailey[1,†], M. Vallikivi[2], M. Hultmark[2] and A. J. Smits[2,3]

[1]Department of Mechanical Engineering, University of Kentucky, Lexington, KY 40506, USA

[2]Department of Mechanical and Aerospace Engineering, Princeton University, Princeton, NJ 08544, USA

[3]Department of Mechanical and Aerospace Engineering, Monash University, VIC 3800, Australia

(Received 16 August 2013; revised 10 April 2014; accepted 12 April 2014;
first published online 14 May 2014)

Five separate data sets on the mean velocity distributions in the Princeton University/ONR Superpipe are used to establish the best estimate for the value of von Kármán's constant for the flow in a fully developed, hydraulically smooth pipe. The profiles were taken using Pitot tubes, conventional hot wires and nanoscale thermal anemometry probes. The value of the constant was found to vary significantly due to measurement uncertainties in the mean velocity, friction velocity and the wall distance, and the number of data points included in the analysis. The best estimate for the von Kármán constant in turbulent pipe flow is found to be 0.40 ± 0.02. A more precise estimate will require improved instrumentation.

Key words: turbulent boundary layers, turbulent flows

1. Introduction

For wall-bounded flows over a smooth wall (assuming that the convection terms are negligible), we can express the mean velocity variation in the so-called overlap region in either inner scaling according to

$$U^+ = \frac{1}{\kappa} \ln y^+ + B, \tag{1.1}$$

or in outer scaling as in

$$U_{cl}^+ - U^+ = -\frac{1}{\kappa} \ln \frac{y}{R} + B^*. \tag{1.2}$$

This result has classically been found through similarity hypotheses (von Kármán 1930), mixing length concepts (Prandtl 1925), asymptotic matching (Millikan 1938), dimensional analysis (cf. Buschmann & Gad-el Hak 2007) or, more recently, high-Reynolds-number asymptotic analysis (George & Castillo 1997; Jiménez & Moser 2007). Here, U is the mean streamwise velocity, $U^+ = U/u_\tau$, $y^+ = yu_\tau/\nu$, $u_\tau = \sqrt{\tau_w/\rho}$, τ_w is the wall stress, ρ is the fluid density and ν is the kinematic viscosity of

† Email address for correspondence: scbailey@engr.uky.edu

the fluid. Furthermore, $U_{cl}^+ = U_{cl}/u_\tau$, where U_{cl} is the mean velocity on the centreline and R is the radius of the pipe. Using (1.1) and (1.2), we can also write

$$U_{cl}^+ = \frac{1}{\kappa} \ln R^+ + B + B^*. \tag{1.3}$$

The von Kármán constant κ and the additive constants B and B^* were originally thought to be universal. Reviews of experimental data by Coles (Coles 1956; Coles & Hirst 1968) led to the values of $\kappa = 0.40$–0.41 being generally accepted, and the values $\kappa = 0.41$, $B = 5.2$ and $B^* = 0.65$ became commonly cited (Huffman & Bradshaw 1972; Bradshaw & Huang 1995; Schlichting & Gersten 2000). More recent experiments, however, have suggested that these constants could depend on the flow under consideration (Nagib & Chauhan 2008), or that the convection terms present in boundary layers act to alter the velocity profile compared to fully developed channel and pipe flows where they are strictly zero, appearing as a change in the constants (George 2007). For example, in turbulent boundary layers, Österlund *et al.* (2000) found $\kappa = 0.384$, $B = 4.17$ and $B^* = 3.6$, while measurements in channel flows made by Zanoun, Durst & Nagib (2003) indicated $\kappa = 0.37$ and $B = 3.7$. In pipe flow, McKeon *et al.* (2004*a*) found $\kappa = 0.421$, $B = 5.60$ and $B^* = 1.20$, whereas Monty (2005) reported $\kappa = 0.386$ in a different pipe facility (and at lower Reynolds number). Zanoun *et al.* (2003) pointed out that values of κ from 0.33 to 0.43 and B from 3.5 to 6.1 have been proposed, with no apparent convergence in time. A more recent review, together with a historical perspective on logarithmic mean flow scaling and the associated constants, is provided by Örlü, Fransson & Alfredsson (2010).

Many of these estimates of κ were based on regression fits to (1.1) or its derivative, which can easily lead to bias errors, especially when the lower and upper limits of the logarithmic region are still being debated (see e.g. Marusic *et al.* 2010; Smits, McKeon & Marusic 2011). To avoid such errors for pipe flow, additional means for obtaining κ were employed by Zagarola & Smits (1998) and McKeon *et al.* (2004*a*). One way, based on integrating (1.1) from the wall to the centreline and assuming complete similarity of the mean velocity profile, uses the Reynolds-number dependence of the friction factor $\lambda = 8(u_\tau/\overline{U})^2$, where $\overline{U}$ is the area-weighted bulk velocity (for details, see Zagarola & Smits 1998). With $Re_D = 2\overline{U}R/\nu$, the friction law gives

$$\frac{1}{\lambda^{1/2}} = \frac{1}{2\kappa\sqrt{2}\log e} \log(Re_D \lambda^{1/2}) + C, \tag{1.4}$$

where C is an empirical constant. Note that (1.3) and (1.4) are equivalent if U_{cl}^+ and $\overline{U}^+$ differ by a constant. For pipe flow, this approach has the advantage that u_τ can be found with high precision by measuring the pressure drop along the pipe, and so (1.4) can give an alternative estimate of κ.

Despite these precautions, the pipe flow results of Zagarola & Smits (1998) and McKeon *et al.* (2004*a*) have been disputed, including arguments that the Pitot profiles required a turbulence correction (Perry, Hafez & Chong 2001; Nagib & Chauhan 2008). Such disputes could not be addressed without complementary thermal anemometry measurements made in the same facility, which have since been obtained. Five complete data sets now exist on the mean velocity distribution in the Princeton University/ONR Superpipe at Reynolds numbers ranging across $81 \times 10^3 \leqslant Re_D \leqslant 1.8 \times 10^7$. These profiles were taken using Pitot tubes, conventional hot wires and nanoscale thermal anemometry probes (NSTAPs). Here, we aim to use these data to establish the best estimate for the value of von Kármán's constant for the flow in a hydraulically smooth pipe, together with its uncertainty levels.

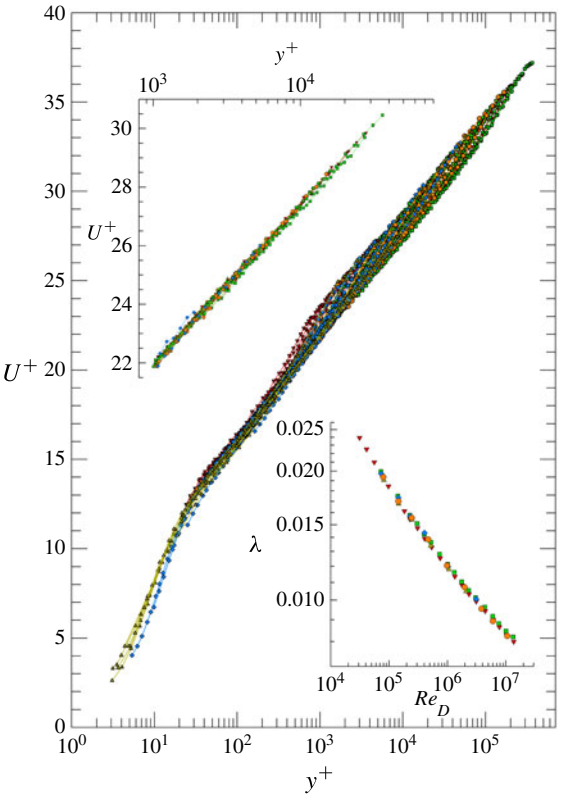

FIGURE 1. (Colour online) Comparison of all mean velocity profiles included in the current study: ▽, ZS; □, MLJMS; ◇, MMJS; ○, VS; and △, HVBS. Inset upper left: only data points falling in the range $1000 < y^+ < 0.1R^+$. Inset lower right: friction factor dependence on Re_D for all data sets.

2. Experimental data

The five data sets on the mean velocity in the Superpipe are the following: the Pitot data of Zagarola & Smits (1998) (denoted ZS) and McKeon *et al.* (2004*a*) (denoted MLJMS); the conventional hot-wire data of Morrison *et al.* (2004) (denoted MMJS), whose mean flow results taken with hot-wire probes of sensing length of 500 and 250 μm have not previously been published; the 60 μm sensing length nanoscale thermal anemometry probe (Bailey *et al.* 2010; Vallikivi & Smits 2014) results of Hultmark *et al.* (2012, 2013) (denoted HVBS); and a new Pitot data set Vallikivi (2014) acquired specifically for the present study (denoted VS). A comparison of mean velocity profiles and Re_D dependence of λ from all data sets is provided in figure 1.

The Superpipe is a closed-return facility, designed to produce high-Reynolds-number pipe flow through pressurizing the working fluid, and it is described in detail by Zagarola (1996) and Zagarola & Smits (1998). In all studies, the test pipe used was the same pipe used by Zagarola & Smits (1998), with $R = 64.68$ mm and relative roughness of $k/R = 2.3 \times 10^{-6}$, being hydraulically smooth for $R^+ < 2.17 \times 10^5$ ($Re_D < 13.5 \times 10^6$) (McKeon 2003; McKeon *et al.* 2004*a*). Prior to the HVBS and VS experiments, the test pipe was disassembled to accommodate rough pipe experiments, and then reassembled using optical inspection of every connection to

minimize mismatches between sections. The measurement station in all cases was located $392R$ downstream from the entrance to the pipe, to assure fully developed flow. The streamwise pressure gradient in the pipe was measured with 17 pressure taps over a distance of $50R$ to obtain the friction velocity, u_τ. The particular flow conditions for each data set are given in the appropriate references, where further descriptions of each experiment may also be found. For the present analysis, to avoid any potential biasing by surface roughness effects, ZS and MLJMS data for $R^+ > 2.17 \times 10^5$ ($Re_D > 13.5 \times 10^6$) have been excluded. In addition, the $Re_D = 6 \times 10^6$ data from MMJS and HVBS experienced relatively large temperature changes, resulting in anemometer drift, and so have also been excluded. Finally, the $Re_D = 5.5 \times 10^4$ case of MMJS was excluded due to errors identified in the probe calibration data (Hultmark, Bailey & Smits 2010). It was found that the measured R^+ was found to be within 3 % of $0.0655Re_D^{0.9125}$ for the range of Reynolds numbers considered here.

For the VS experiments, reported here for the first time, a Pitot tube with 0.40 mm diameter was used and the static pressure was measured using two 0.40 mm static pressure taps located in the pipe wall. This Pitot diameter was comparable to the 0.89 mm and 0.30 mm diameter Pitot tubes used by Zagarola (1996) and McKeon (2003) respectively, and was equal to $0.006R$ or approximately 1000 viscous lengths at the highest Reynolds number measured. The pressure difference was measured using a Datametrics 1400 transducer with a 2488 Pa range for all atmospheric pressure cases, and Validyne DP15 transducers with ranges 1379, 8618, 34 474 and 82 737 Pa for the pressurized cases, depending on the pressure. For the streamwise pressure gradient measurements, a 133 Pa MKS Baratron transducer was used for atmospheric cases and a 1333 Pa MKS transducer or Validyne DP15 34 474 Pa transducer was used for pressurized cases. All pressure transducers were calibrated prior to use. For calibrating the lowest pressure range, a liquid manometer with uncertainty of less than ± 0.40 % of the reading was used, whereas for the intermediate-range Validyne transducers an Ametek pneumatic dead-weight tester was used with accuracy of ± 0.05 %. The tunnel pressure was measured using Validyne DP15 transducers with 345, 3447 and 27 579 kPa ranges, and these were calibrated using an Amthor dead-weight pressure gauge tester with accuracy of ± 0.1 % of the reading.

Data were acquired at $Re_D \approx 80 \times 10^3$, 150×10^3, 250×10^3, 500×10^3, 1×10^6, 2×10^6, 4×10^6, 6×10^6 and 10×10^6, with the Superpipe pressurized for $Re_D \geqslant 150 \times 10^3$. The initial distance between the wall and the probe, y_0, was determined by using a depth measuring microscope (Titan Tool Supply Inc.). To position the probe, a stepper motor traverse was used equipped with a linear optical encoder with a resolution of 0.5 μm (SENC50 Acu-Rite Inc.).

All Pitot data sets (ZS, MLJMS, VS) were processed using the static tap and shear corrections proposed by McKeon & Smits (2002) and McKeon *et al.* (2003), with the additional turbulence correction and associated near-wall correction discussed by Bailey *et al.* (2013). As done by McKeon *et al.* (2004*a*), we discard Pitot data from measurement points lying less than two probe heights from the surface. To estimate the turbulence intensity required for applying the turbulence correction, the streamwise turbulence intensity of HVBS is used for $Re_D \leqslant 6 \times 10^6$. For Pitot cases at higher Reynolds numbers, the turbulence intensity was estimated by assuming that the logarithmic scaling observed by HVBS was valid throughout the layer.

A comparison of the newly acquired VS Pitot data set to the HVBS NSTAP data set taken at the same Reynolds numbers is provided in figure 2. The results demonstrate the negligible difference between the two measurement techniques, after all applicable corrections have been applied.

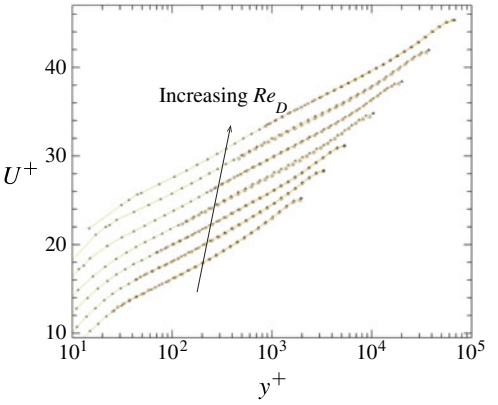

FIGURE 2. (Colour online) Comparison of VS Pitot (○) and HVBS (△) mean velocity profiles at $Re_D = 80 \times 10^3$, 150×10^3, 250×10^3, 500×10^3, 1×10^6, 2×10^6 and 4×10^6. Note that successive Reynolds numbers are shifted vertically by $2u_\tau$ for clarity.

The fitting of (1.1), (1.3) and (1.4) to the data was conducted using the linearized form of the equations applying a least-squares approach (implemented through the MATLAB function *polyfit*). The fit to (1.1) therefore returned κ^{-1} and B; to (1.3) it returned κ^{-1} and $(B + B^*)$; and to (1.4) it returned $(2\sqrt{2}\kappa \log e)^{-1}$ and C_2. For fitting to (1.3), U_{cl}^+ was determined by a cubic fit to the three data points straddling the centreline, although there was a negligible difference when compared to the same estimate using the measurement point located at the pipe centreline.

Estimates for the experimental uncertainties used in the uncertainty analysis are listed in table 1. In most cases, given that much of the facility and instrumentation used was largely unchanged, these follow the values provided by ZS. Additional sources of bias error are discussed in appendix A, and the approach used to estimate the uncertainty in κ is described in appendix B.

3. The von Kármán constant as determined from the mean velocity profile

We first find κ using a least-squares fit of (1.1) to each individual velocity profile within the range $y^+ > 1000$ to $y/R < 0.1$. These values were selected to ensure that the fit was unambiguously contained within the range where a log law is expected to hold, and our choice is not meant to suggest a particular range of validity of the logarithmic scaling.

The results are presented in figure 3(*a*) and suggest a Reynolds-number-independent value of κ, but with large variations in experimental uncertainty across the Reynolds-number range and between measurements. Note that, with regards to uncertainty, there appears to be no advantage to using either thermal anemometry or Pitot tube measurement approaches, because the largest uncertainty is associated with the smallest number of data points falling within the acceptance range and used for the regression fit. Thus, the uncertainty levels generally decrease with increasing Re_D. The exception is the early data set of ZS, where the higher uncertainty levels are mostly due to the relatively large Pitot probe used by ZS, so that fewer measurement points fall within the fitting range. The most likely values for κ vary considerably among the data sets. For the earlier Pitot probe profiles, the ZS values lie between 0.39 and 0.43, while the MLJMS data set suggests 0.40–0.42 (consistent with the previous estimate of 0.421 (McKeon *et al.* 2004*a*) at high Reynolds number). Both thermal

Data set	ZS		MLJMS		MMJS		HVBS		VS	
Source	Bias	Prec.	Bias	Prec.	Bias	Prec.	Bias	Prec.	Bias	Prec.
Pitot differential (%)	±0.4	±0.8 [a]	±0.4	±0.6 [a]	N/A		N/A		±0.4	0.8 [a]
Pitot corrections (%)	±1 [b]	±0.3 [c]	±1 [b]	±0.3 [c]	N/A		N/A		±1 [b]	0.3 [c]
Hot-wire precision (%)	N/A		N/A		±0	±0.4 [a]	±0	±0.4 [a]	N/A	
Hot-wire calcn. (%)	N/A		N/A		±1	±0	±1	±0	N/A	
Anemometer drift (%)	N/A		N/A		±1	±0	±1	±0	N/A	
y position (μm)	118	5	41	5	41	5	5.25	0.5	13.25	0.5
Tunnel pressure (%)	±0.3		±0.3		±0.3		±0.3		±0.3	
Pressure gradient (%)	±(0.17–0.83)		±(0.17–0.83)		±(0.17–0.68)		±(0.17–0.68)		±(0.17–0.68)	
Temperature (%)	±0.05		±0.05		±0.05		±0.05		±0.05	
Dynamic viscosity (%)	±0.8		±0.8		±0.8		±0.8		±0.8	
Pipe radius (%)	±0.06	±0	±0.06	±0	±0.06	±0	±0.06	±0	±0.06	±0

TABLE 1. Bias and precision uncertainty estimates. Where a single value is stated across both bias and precision columns, the same value was used for both bias and precision uncertainty. (a) Value estimated from data scatter. (b) Value estimated based on results of Bailey *et al.* (2013). (c) Value estimated from scatter in measured velocity gradient.

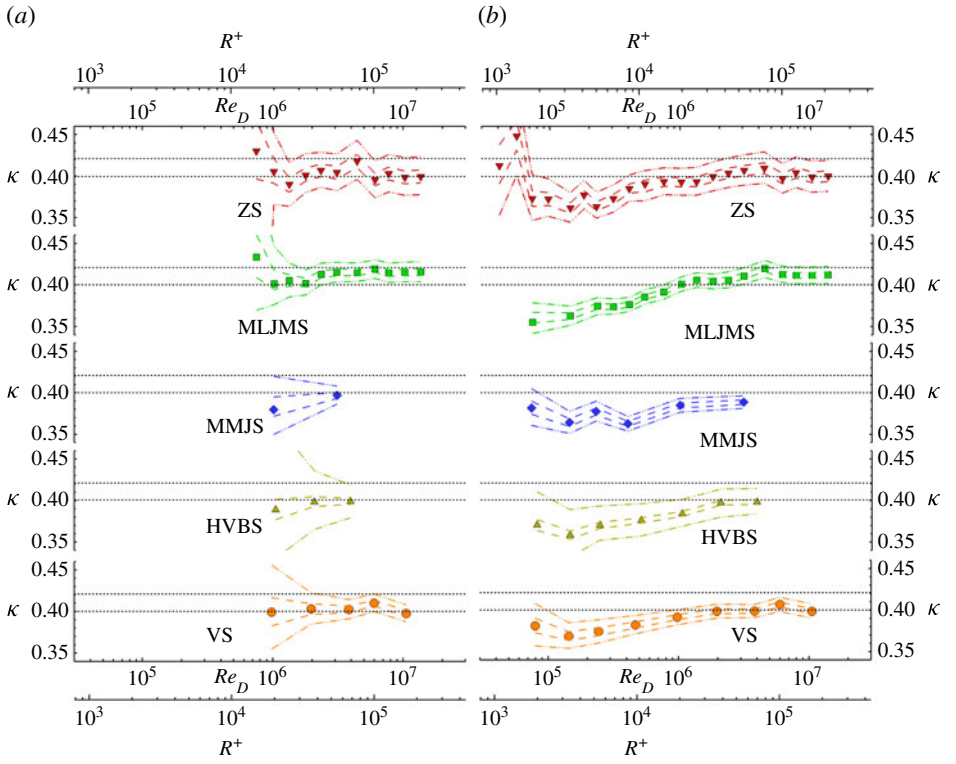

FIGURE 3. (Colour online) Value of κ as estimated from least-squares fit of (1.1) to the mean velocity profiles measured at different Reynolds numbers for the range of data points lying in the range (*a*) $1000 < y^+ < 0.1R^+$ and (*b*) $3(R^+)^{1/2} < y^+ < 0.15R^+$. Dot-dot-dashed lines indicate 95 % confidence limits, and dashed lines indicate 50 % confidence limits. Horizontal black dotted lines indicate the values of $\kappa = 0.40$ and $\kappa = 0.421$.

anemometry cases give estimates of κ varying between 0.38 and 0.40, whereas the most recent Pitot data set indicates a value between 0.40 and 0.41.

In addition to the conservative range ($y^+ > 1000$ to $y/R < 0.1$), we also considered the overlap layer range of $3(R^+)^{0.5} < y^+ < 0.15R^+$ used by Marusic *et al.* (2013) based on the estimate by Klewicki, Fife & Wei (2009) of the range $y^+ \geqslant 2.6(R^+)^{0.5}$ where viscous force loses leading-order influence. The resulting estimate of κ was found to be Reynolds-number-dependent for $Re_D \lesssim 2 \times 10^6$, as shown in figure 3(*b*). Note that $y^+ = 3(R^+)^{0.5} \approx 600$ at $Re_D \approx 2 \times 10^6$, corresponding to the lower limit observed by McKeon *et al.* (2004*a*). Above this Reynolds number, the values of κ estimated become very close for the two different limits. Virtually identical results were observed when the upper limit was reduced to $y/R = 0.1$, suggesting that the Reynolds-number dependence is caused by the R^+ dependence of the lower limit. Therefore, the current results do not support the Reynolds-number-dependent lower limits used by Marusic *et al.* (2013).

4. The von Kármán constant as determined from Reynolds-number dependence of bulk properties

Although regression fits to the mean velocity profiles can provide an estimate of κ, the procedure is sensitive to the range of y^+ values selected for fitting, and to small

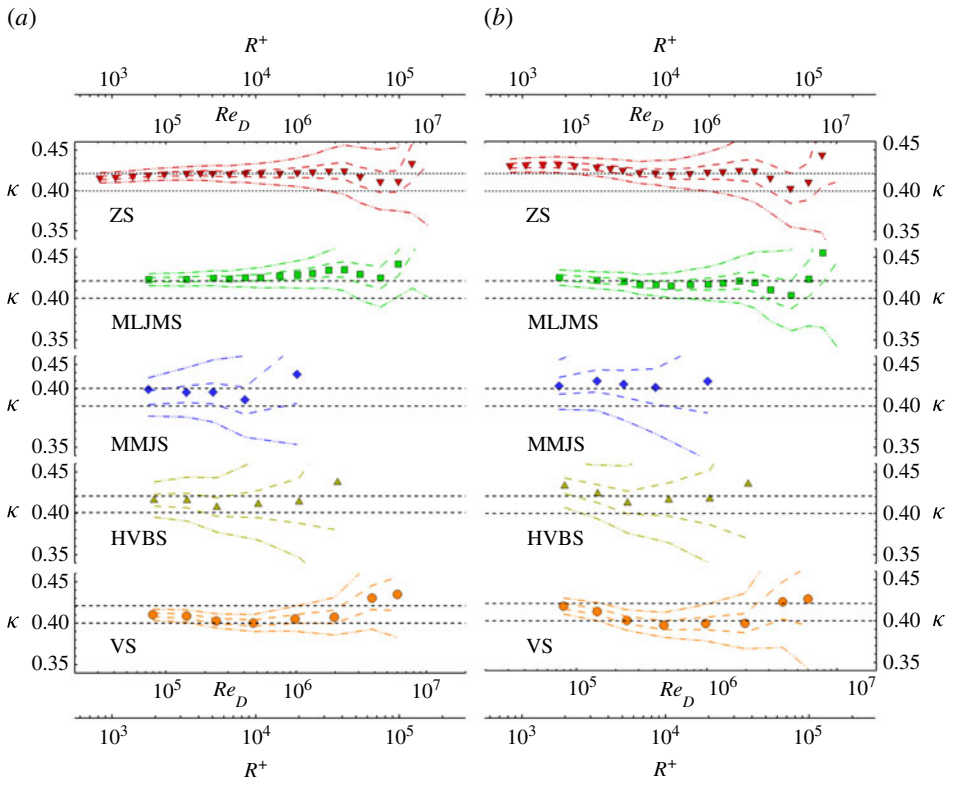

FIGURE 4. (Colour online) Value of κ estimated from least-squares fit of (*a*) equation (1.4) (friction factor fit) and (*b*) equation (1.3) (centreline velocity fit) shown as a function of the lowest Reynolds-number case used for the regression fit. Dot-dot-dashed lines indicate 95 % confidence limits, and dashed lines indicate 50 % confidence limits.

errors in u_τ (see e.g. Örlü *et al.* 2010). However, for pipe flow a valid estimate of κ must satisfy (1.1), (1.2), (1.3) and (1.4). Therefore, given a sufficient Reynolds-number range, one can also estimate κ from the Reynolds-number dependence of the bulk flow properties. This was the approach taken by Zagarola & Smits (1998) and McKeon *et al.* (2004*a*).

Figure 4 shows the value of κ estimated by fitting (1.4) and (1.3) to the centreline velocity data and the friction factor data, respectively. The results are shown as a function of the lowest Reynolds number included in the fit. For example, for the highest Reynolds number shown, κ was estimated from fitting only the two highest Reynolds-number cases; each successively lower Reynolds-number data point on the figure represents the results from a curve fit with one additional point included in the fit. Hence the lowest Reynolds number plotted represents the estimate of κ determined from fitting the entire data set.

As noted by McKeon *et al.* (2004*a*) with respect to the MLJMS data set, we see that for $Re_D > 300 \times 10^3$ the estimates for all data sets become Reynolds-number-independent, except for the highest Reynolds-number values, where the number of points in the fit is reduced and the uncertainty increases significantly. For $Re_D > 300 \times 10^3$, fitting (1.4) or (1.3) gives similar values, although the latter estimate is subject to slightly higher uncertainty because it relies on a single measurement of U_{cl}^+ at each

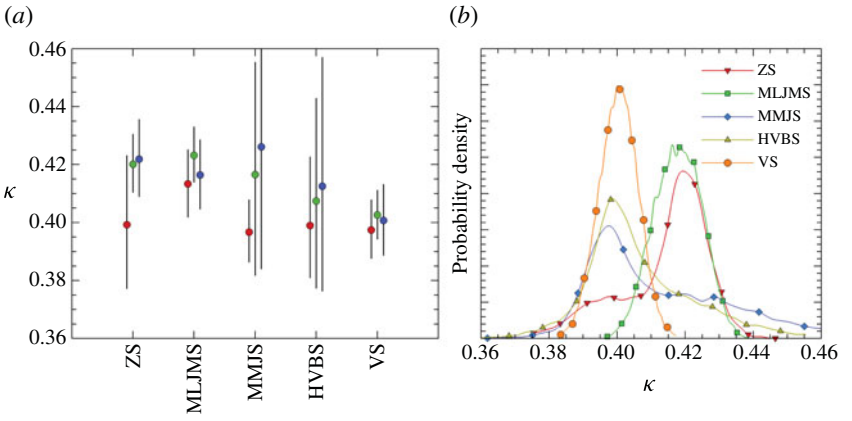

FIGURE 5. (Colour online) (*a*) Values of κ estimated from each data set with error bars indicating 95 % confidence interval. For each data set, the value on the left is obtained from the regression fit to (1.1); the one in the centre is from the regression fit to (1.3); and the one on the right is from the regression fit to (1.4). (*b*) Probability density functions of κ for each data set found by combining the uncertainty of all three estimates.

Reynolds number. The ZS, MLJMS and MMJS data sets return a value of $\kappa \approx 0.42$ consistent with the McKeon *et al.* (2004*a*) estimate of $\kappa = 0.421$. However, the more recent HVBS and VS data indicate $\kappa \approx 0.41$ and 0.40, respectively. In addition, we see that the uncertainties in the thermal anemometry data sets are much higher than that of the Pitot data sets, primarily because the thermal anemometry data cover a smaller and lower Reynolds-number range. A fit of (1.4) was also applied to the high-Reynolds-number friction factor data of Swanson *et al.* (2002) (tabulated in McKeon *et al.* 2004*b*). The resulting estimate of κ was found to depend strongly on the Reynolds-number range selected for the fit, varying between 0.41 and 0.5.

5. Discussion

The different estimates of κ from each data set are summarized in figure 5. For the regression fit to (1.1), we use the value determined from the highest Reynolds-number case, where the uncertainty is lowest due to the number of data points in the logarithmic region. For the estimates determined from regression fits to (1.3) and (1.4), we use the value determined from fitting to $Re_D > 3 \times 10^5$, which comprises the range where the estimate becomes Re_D-independent and the uncertainties are lowest due to the number of data points included in the fit.

If we assume that the log law is valid, then (1.1), (1.3) and (1.4) must be simultaneously valid, and inspection of figure 5(*a*) reveals two important points. First, no single value of κ is within the 95 % uncertainty bounds of all five data sets. This indicates that one or more sources of uncertainty remain undetected while also reflecting the difficulty inherent in determining κ experimentally. Second, the estimates obtained by fitting equations (1.3) and (1.4) are consistently higher than those obtained by fitting (1.1), suggesting that these undetected errors are consistently biasing the estimate.

Many factors contribute to the overall uncertainty, but the primary ones are the estimate of y_0, the method chosen to integrate the mean velocity profile near the wall in order to find $\overline{U}$, drift in the thermal anemometry measurements, and turbulence

corrections to the Pitot probe data (see appendix A). For example, the turbulence correction influences the value of κ obtained by fitting (1.1) by 2 %, and a relatively small (0.08 % of R) uncertainty in the wall distance can change κ by up to 3 %, whereas estimates obtained by fitting equations (1.3) and (1.4) are nearly unaffected by these factors. On the other hand, the estimates obtained using (1.3) and (1.4) are very sensitive to the different pressure transducers used to obtain the velocity and pressure gradient, as well as the integration methods for estimating bulk properties. Estimates obtained from the hot-wire data are extremely sensitive to any type of drift, where estimates obtained using (1.3) and (1.4) can be influenced by up to 6 % even with high-quality calibrations with less than 1 % drift. Overall, it can be seen that there is no measurement technique or method of analysis that could be identified as the most precise.

Although the 95 % confidence intervals indicate that no value of κ is supported by all data sets, within each data set there exists a range of possible values, following the assumption that (1.1), (1.3) and (1.4) must be simultaneously valid. Thus ZS indicates $0.41 < \kappa < 0.42$; MLJMS indicates $0.41 < \kappa < 0.43$; MMJS indicates $0.39 < \kappa < 0.41$; HVBS indicates $0.39 < \kappa < 0.41$; and VS indicates $0.39 < \kappa < 0.41$. However, since these ranges represent an overlap of three separate 95 % confidence ranges, the confidence of κ lying within this range for each data set is actually lower. This is demonstrated by the probability density functions (p.d.f.s) shown in figure 5(*b*), which were compiled from combining all three methods used to estimate κ using the uncertainty analysis described in appendix B. We see that the most probable value of κ is 0.40 for the three most recent data sets, arising from reduced uncertainty in the fitting of (1.1) at high Reynolds numbers combined with the higher uncertainty in fitting equations (1.3) and (1.4) for these data sets. Conversely, the ZS and MLJMS data sets indicate the most probable value of κ is 0.42 due to the agreement between the fits of (1.3) and (1.4) (and reduced uncertainty) for these data sets.

Using these p.d.f.s, it can also be determined that the confidence of κ being within the intervals of overlap in 95 % confidence for the three techniques is approximately 50 % or less for the ZS, MLJMS, MMJS and HVBS data sets (i.e. a 50 % chance that $0.41 < \kappa < 0.42$, $0.41 < \kappa < 0.43$, $0.39 < \kappa < 0.41$ and $0.39 < \kappa < 0.41$, respectively). In comparison the agreement between the three estimates of κ for the VS data set results in a 73 % confidence that $0.394 < \kappa < 0.408$, indicating that this data set is the one least affected by undetected bias errors.

As previously noted, this disagreement between the multiple estimates of κ cannot be accounted for using the known bias and precision errors provided in table 1, suggesting the presence of undetected bias errors. For obvious reasons, it is not possible to identify the source of these undetected errors. However, examining all data sets as a whole does reveal symptoms of these errors, which provide further information that can be used to assess the data. We start first by noting that (1.4) can be rewritten as

$$\overline{U}^+ = \frac{1}{\kappa} \ln R^+ + B + B^* + E, \tag{5.1}$$

where $E = U^+_{cl} - \overline{U}^+$, which includes contributions from the difference between the actual velocity profile and (1.1) extrapolated to the wall and to the core region. As noted by Zagarola & Smits (1998), the difference between the true velocity profile and (1.1) near the wall is Reynolds-number-dependent but, for a fixed lower limit of the overlap layer, should vanish when R^+ is large. Hence, assuming no Reynolds-number dependence in the wake contribution to $\overline{U}^+$ and constant B^*, at sufficiently high R^+, E should also be constant. We examine this Reynolds-number dependence in figure 6.

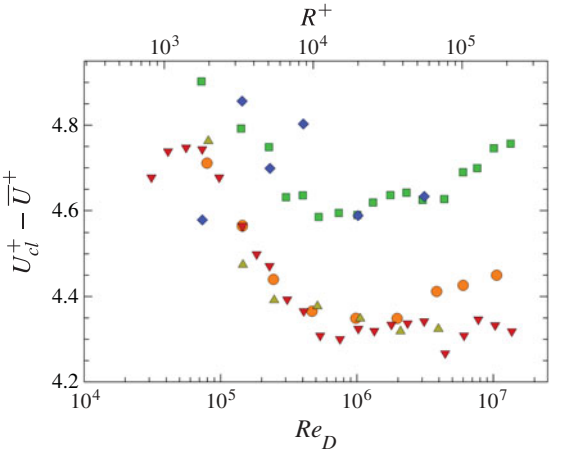

FIGURE 6. (Colour online) Reynolds number dependence of $E = U_{cl}^+ - \overline{U}^+$: ▽, ZS; □, MLJMS; ◇, MMJS; ○, VS; and △, HVBS.

All data sets demonstrate Reynolds-number dependence in E for $Re_D < 300 \times 10^3$, consistent with the Reynolds-number dependence previously observed when estimating κ from bulk flow properties. For $Re_D > 300 \times 10^3$ the ZS and HVBS data sets appear Reynolds-number-independent whereas the MLJMS and VS data set exhibit Re_D dependence for $Re_D > 3 \times 10^6$. This Reynolds-number dependence at high Reynolds numbers could be due to a Reynolds-number-dependent experimental bias impacting E, as would appear, for example, through the integration of U with insufficient resolution near the wall as discussed in § A.3. However, given the agreement with the VS Pitot and NSTAP, and that the Reynolds-number dependence is not evident on the ZS data set, which was acquired with an even larger Pitot tube, we cannot conclusively attribute the Reynolds-number dependence exclusively to the use of Pitot probes and thus also cannot discount the possibility that the observed Reynolds-number dependence could be due to a real phenomenon, such as a Re_D-dependent inner limit of the overlap region.

Also clearly evident in figure 6 is a shift in E for the MLJMS and MMJS data sets with respect to the other four data sets. These two data sets are also the ones with the greatest disparity between κ estimated from (1.3) and (1.4). The source of this shift in E becomes apparent when closely examining the Reynolds-number dependence of $\overline{U}^+$ and U_{cl}^+, as done in figure 7(*a*,*b*). In these figures, $1/0.4 \ln R^+$ has been subtracted from the values to de-trend the Reynolds-number dependence in a way that would result in a constant value if $\kappa = 0.4$. It is clear by comparison of figures 7(*a*) and (*b*) that the shift in E for the MLJMS and MMJS data sets arises from a bias introduced into the estimate of $\overline{U}$. It is not possible to identify where this bias enters into the estimate, although the Reynolds-number independence of this bias suggests that it is not due to error in y_0.

The bias observed in the MLJMS and MMJS area-averaged data suggests that the κ estimated via (1.3) is a more reliable estimate. However, close examination of figure 7(*b*) shows some interesting behaviour. As noted previously, when plotted in this way, a constant value of $U_{cl}^+ - 1/0.4 \ln R^+$ would occur if $\kappa = 0.4$. As expected from the previous discussion, this is only the case over the entire range $Re_D > 300 \times 10^3$ for the VS (and possibly the HVBS) results. However, within the

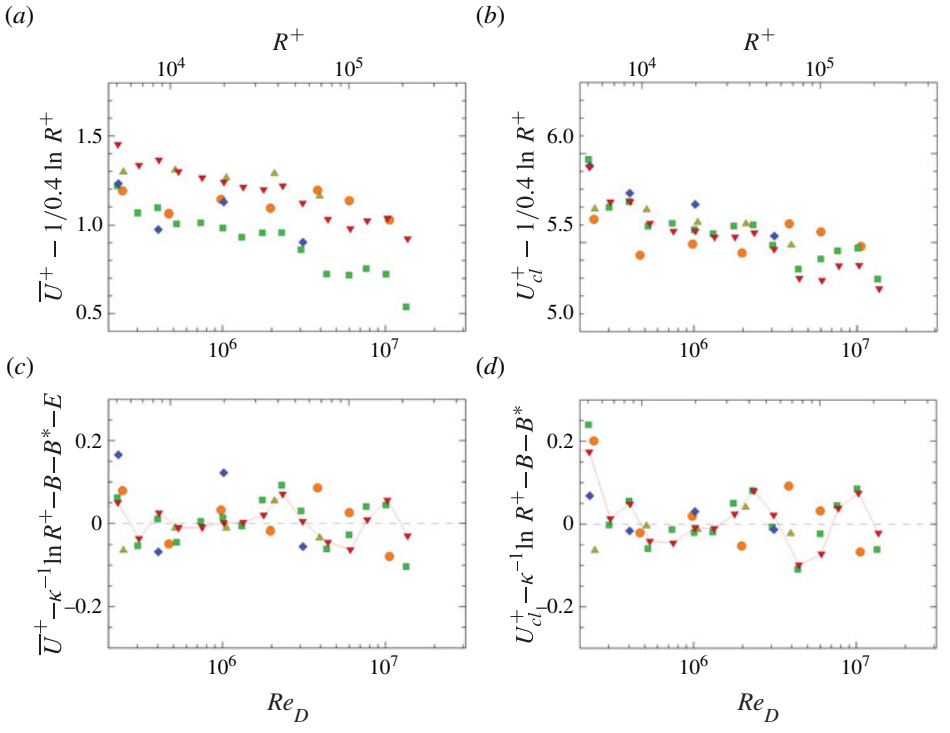

FIGURE 7. (Colour online) (*a*,*b*) Reynolds-number dependence of (*a*) $\overline{U}^+$ and (*b*) U_{cl}^+. (*c*,*d*) Residuals of the curve fits used to find κ shown in figure 5 using (1.4) and (1.3) respectively: ▽, ZS; □, MLJMS; ◇, MMJS; ○, VS; and △, HVBS.

range $300 \times 10^3 < Re_D < 3 \times 10^6$, all data sets follow the same trend. Only for $Re_D > 3 \times 10^6$ is there Reynolds-number dependence in the ZS and MLJMS data sets, which both contain a noticeable shift in value. This shift is also evident in figure 7(*a*).

The similarity in Re_D dependence exhibited in figures 7(*a*) and (*b*) between the ZS and MLJMS data sets is explored in greater detail in figures 7(*c*) and (*d*), which display the residuals of the curve fits to (1.3) and (1.4) that were used to determine the values of κ shown in figure 5. If the experimental errors are random and normally distributed, then these residuals should also be approximately normal with mean of zero. For each individual data set, this appears to be the case. However, the residuals for the ZS, MLJMS and possibly the HVBS data sets all exhibit the same Reynolds-number-dependent behaviour, indicating the presence of a Re_D-dependent bias within the experiments. The presence of this bias indicates that the values of κ found by fits to (1.3) and (1.4) are unreliable. The most likely source of this bias is the use of different pressure transducers with differing sensitivity, which is required to cover the large Reynolds-numbers range of these measurements. As discussed in § A.5, a slight difference in error between these transducers can introduce significant errors in κ estimated using (1.3) and (1.4). However, this variability between transducers will not produce a similar bias in κ estimated from (1.1).

Thus, considering only the estimate of κ using (1.1), we conclude that $\kappa = 0.40$, with the MLJMS data set as an outlier. Furthermore, if we consider the single VS

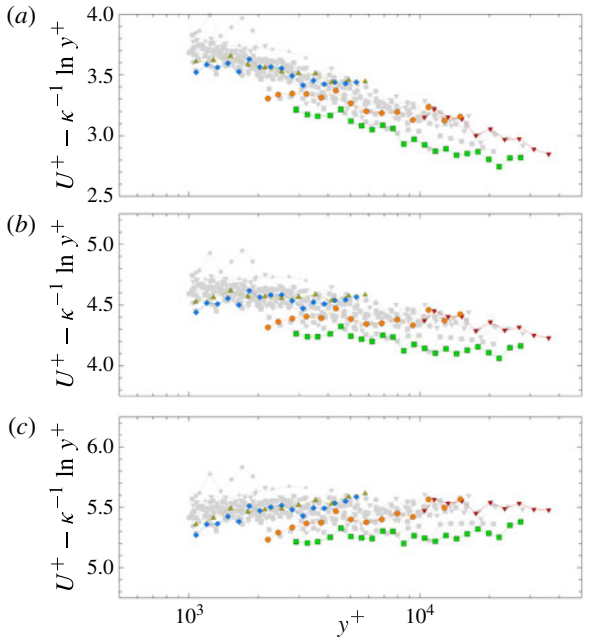

FIGURE 8. (Colour online) Plots of $U^+ - \kappa^{-1} \ln y^+$ within the range $1000 < y^+ < 0.1R^+$ for (*a*) $\kappa = 0.38$, (*b*) $\kappa = 0.40$ and (*c*) $\kappa = 0.42$: $\triangledown$, ZS; $\square$, MLJMS; $\diamond$, MMJS; $\circ$, VS; and $\triangle$, HVBS. Highlighted profiles are the highest Reynolds-number profiles for each data set.

data set, we could therefore conclude that $\kappa = 0.40 \pm 0.01$. However, doing so would necessarily assume that only this data set was free of undetected bias errors, which affected all previous data sets. Such filtering of data sets, although not completely arbitrary, is not prudent, and therefore we must consider the complete collection of data. The lack of consensus suggests that the actual uncertainty in κ is likely to be higher than that given by any single data set, and a more conservative estimate is $\kappa = 0.40 \pm 0.02$. The profiles in the range $1000 < y^+ < 0.1R^+$ are compared to this range of κ in figure 8, in which the logarithmic region should appear constant and equal to B over the entire overlap layer. The results for $\kappa = 0.40$ in figure 8(*b*) suggest a value of $B = 4.5 \pm 0.3$ when $\kappa = 0.40$.

An apparent Reynolds-number-dependent trend in B can also be discerned in figure 8(*b*), reminiscent of the expected behaviour caused by the onset of roughness effects. However, as demonstrated in figure 9(*a*), which shows the value of B determined by fixing $\kappa = 0.40$, this trend is also the same as that observed in figures 7(*a*) and (*b*) and already attributed to bias error. The similarity of the trends in figures 8 and 7(*b*) is not unexpected given the interrelationship between (1.1) and (1.3), and the trend in figure 8(*b*) is thus a manifestation of the same bias error. This is further confirmed in figure 9(*b*), which shows no obvious trend in the value of B produced by the same regression fit to (1.1) that produced the values of κ shown in figure 3(*a*).

Our estimate of $\kappa = 0.40$ is identical to the recent values found for channel flow by Jiménez & Moser (2007) and Schultz & Flack (2013), and the uncertainty limits are consistent with the currently accepted values for boundary layers of $\kappa = 0.38$–0.39

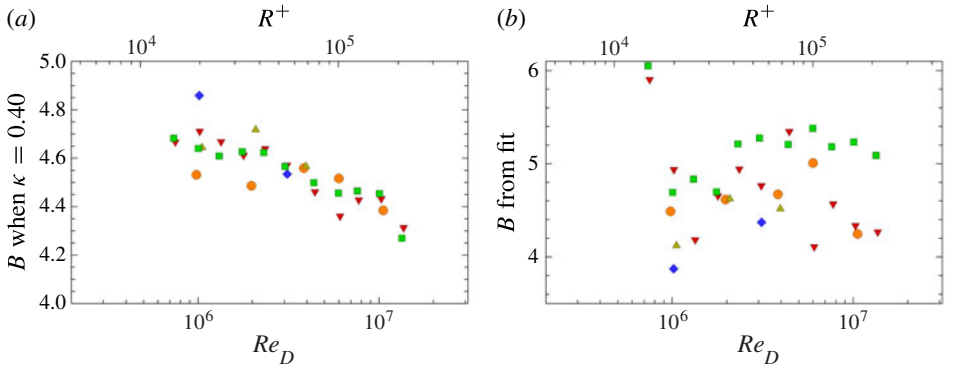

FIGURE 9. (Colour online) Plots of additive constant B determined (a) when κ is fixed at 0.40 and (b) from least-squares fit to (1.1):▽, ZS; □, MLJMS; ◇, MMJS; ○, VS; and △, HVBS.

(Österlund *et al.* 2000; Nagib & Chauhan 2008; Marusic *et al.* 2013). It would appear, therefore, that the present results support the existence of a universal value of κ. However, inspection of figures 8(a) and (c), which show $U^+ - \kappa^{-1} \ln y^+$ for $\kappa = 0.38$ and 0.42, provides little support for the proposed boundary layer value of $\kappa = 0.38$ within the current pipe flow results. It should also be noted that the present results also required a large range of Reynolds number and the use of the most conservative estimate of the logarithmic region to date to obtain a Reynolds-number-independent estimate of κ. To obtain a comparable estimate for turbulent boundary layers and channels would require significantly more data with a Kármán number $>10\,000$ than is currently available (at least for data accompanied by an independent skin friction measurement).

6. Conclusions

For the first time, all available smooth-wall mean flow data sets acquired in the Princeton University/ONR Superpipe were analysed to determine the von Kármán constant, κ, using three different methods. Owing to its large Reynolds-number range and controlled conditions, this facility offers a unique opportunity to estimate the value of κ and its attendant uncertainty.

Unlike most prior studies investigating the value of κ for pipe flow, we do not limit our analysis to a single data set. We find no clear consensus on the value of κ obtained from multiple data sets measured largely independently in the same facility, even following the application of all known corrections and taking into account all the known uncertainties. This suggests that the actual uncertainty in κ is likely to be higher than that given for any single data set studied. Based on all our observations, we therefore estimate the value of κ for high-Reynolds-number pipe flow to be 0.40 ± 0.02. The fact that, even with this facility, using modern instrumentation, the value of κ can only be determined to within this precision is a notable result. In order to obtain a more precise estimate of κ, improved experimental techniques are required, accompanied by carefully conducted experiments and analysis. It should also be noted that evaluation of κ in turbulent boundary layers is even more challenging, given that measurements of u_τ are less accurate. Contrary to what has been suggested in previous work, we found that differences between values of κ cannot be attributed only to the differences between hot-wire anemometry and Pitot tube measurements.

Acknowledgements

This work was supported through ONR grant N00014–09-1-0263 (Program Manager Ronald Joslin). The authors would also like to thank all reviewers for their helpful comments, in particular Referee 4, who suggested looking at the Reynolds-number dependence of the difference between (1.3) and (1.4).

Appendix A. Bias error effects on determination of von Kármán constant

Uncertainties may be divided into bias errors and precision errors. Here, we treat precision uncertainty as the expected variation that would occur amongst repeated measurements of the same quantity as reflected through experimental scatter. Bias error is more difficult to identify and we treat it as a consistent deviation between the measured and true quantities as introduced by the experiment set-up, procedure or analysis. The estimated errors for the data sets under consideration are provided in table 1, where uncertainty values derived from stated manufacturer values are treated as bias error. Here we discuss several additional sources of bias error that can play a role in estimates of κ, and investigate the impact of each source on the estimate.

A.1. *Impact of Pitot probe corrections*

Pitot probe corrections for shear, near-wall, viscous and finite static tap size are discussed in great detail in many sources (see e.g. Tavoularis 2005; Tropea, Yarin & Foss 2007). With the exception of eliminating data points less than two probe diameters from the surface, the complete correction suite used here is described in Bailey *et al.* (2013) and has been demonstrated to result in Pitot measured mean velocity agreeing with that measured by hot wires to within 1 %. This difference therefore can be used as an approximation of the bias error that can be expected in the measured mean velocity. However, the source of this bias should not be considered exclusive to the Pitot and the accuracy of its corrections, but can equally be attributed to uncertainty in the hot-wire mean velocity.

Of particular interest for the Pitot measurements is the magnitude of the correction for turbulence effects, which has previously been observed to significantly bias the estimate of κ found using mean flow profiles (Perry *et al.* 2001; Nagib & Chauhan 2008). To assess the effect of this correction on estimates of κ, we repeated the analysis without the turbulence correction. The effect of not using the turbulence correction was found to be an increase in estimated κ of $+2\,\%$ when determined using (1.1) and bias of $-0.2\,\%$ and $+0.2\,\%$ when using (1.3) and (1.4) respectively.

A.2. *Initial probe position*

The effects of initial probe position are discussed in detail in Örlü *et al.* (2010), which illustrates how accurate determination of wall position is necessary to correctly deduce mean and turbulence quantities. In the Superpipe, the wall layer thickness is 64.68 mm and, at $Re_D = 1.3 \times 10^7$, the viscous length is only 300 nm. Therefore, an inaccurate estimate of wall position can have significant effect on the mean velocity profile. To minimize this zero position error, the ZS data set used a capacitance-based method to determine the zero position to within 40 μm, and the MLJMS data set used electrical contact between the probe and surface to identify initial probe position and cite accuracies of 5 μm. For the MMJS data, no details were available regarding how the initial probe distance was determined. For the HVBS and VS data, initial

probe position was determined via depth measuring microscope, with the zero location marked using an electrical contact, and a 5 μm uncertainty is estimated. Note that these cited values are likely to be underestimates of the true bias, which can arise from error in estimating Pitot probe diameter, probe orientation with respect to the wall, hot-wire probe distortion and rotation relative to the wall plane, the method used to measure wall distance, or the possibility that electrical contact is rarely made at a clearly defined and repeatable point (Hutchins & Choi 2002). These errors are also further compounded in the Superpipe facility due to lack of optical access to the measurement station and therefore inability to verify the relative position of the probe to the wall.

To illustrate how uncertainty can propagate into the estimate of κ, we artificially biased the zero position of the VS data set by +50 μm (12.5 % of the probe diameter, corresponding to a bias of approximately 1.5 viscous units at the lowest Reynolds number and 125 viscous units at the highest Reynolds number). For κ estimated from (1.1), there was a resulting bias in κ of −1 % at $Re_D = 1 \times 10^6$ to −3 % at $Re_D \geqslant 4 \times 10^6$, corresponding to biasing of κ estimates from −0.004 to −0.01. As might be expected, the effect on the estimates of κ using (1.4) and (1.3) were much less dramatic, corresponding to Reynolds-number-dependent bias in κ estimate from −0.01 % to −0.05 % using (1.4) and +0.005 % to +0.05 % using (1.3).

A.3. *Estimate of area-averaged flow velocity from discrete data*

An associated error to that of initial probe position, which could have a noticeable effect on the estimate of κ using (1.4), is the numerical integration scheme used to determine area-averaged velocity to calculate the Reynolds number. As the Reynolds number increases, and the inner layer thins accordingly, there is a potential Reynolds-number-dependent bias introduced into any estimate of area-averaged velocity due to an inability to resolve this high-shear region. This compounds any error introduced by the order of the numerical integration scheme used. In this study, we have used second-order-accurate trapezoidal integration and, where necessary, have extrapolated the profile down to the wall with data measured at lower Reynolds numbers and assuming wall scaling is valid. Not performing this extrapolation process was found to have a surprisingly significant effect on κ determined using (1.4), with a bias in κ of typically +3 %, +0.4 %, +1 % and +1 % being observed by neglecting this step for the ZS, MLJMS, MMJS and VS data sets respectively. For the HVBS data set, the closest measurement point was always within the buffer layer and the extrapolation process was not required.

A.4. *Hot-wire drift*

In hot-wire anemometry, the most sensitive issue in experiments is a proper calibration of the sensor and some drift in the response is an inherent part of the measurements. Even the tiniest drift during measurements can cause significant errors, especially when estimating mean velocities. For the HVBS data, a calibration was conducted at centreline with 14 flow velocities before and after each profile, and agreement of the calibration curves was used as a validation condition for acceptance of the profile. Then all 28 points were combined to fit the calibration curve used for all data processing. In figure 10(*a*) all calibration curves are shown and in figure 10(*b*) the relative difference, U_{rel}, between each pre- and post-measurement calibration and the combined calibration U_{comb} is illustrated (where relative velocity is given as $U_{rel} = (U_{cal} - U_{comb})/U_{comb}$ and relative voltage as $E_{rel} = (E_{cal} - E_{min})/(E_{max} - E_{min})$). It can be seen that, for most cases, the relative difference between calibration curves is below 1 %.

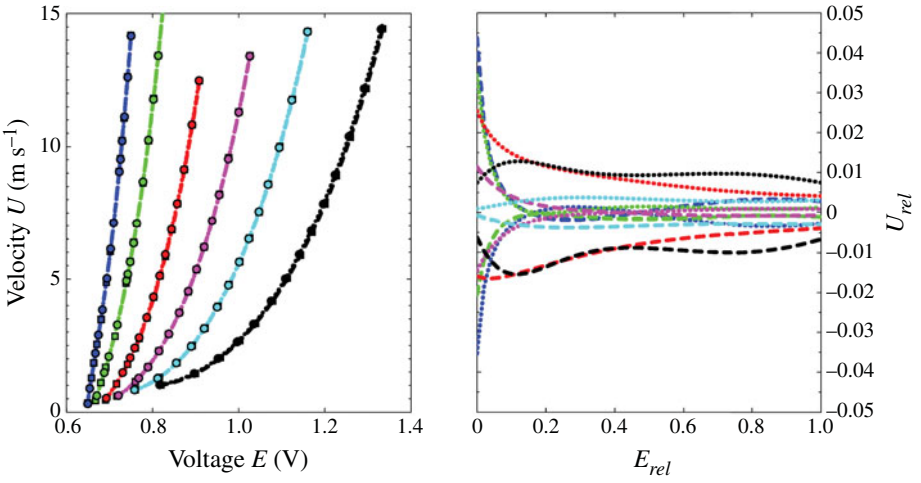

FIGURE 10. (Colour online) Calibration points and curves for all cases in the HVBS data set. Dashed line and circles indicate pre-calibration fit; dotted line and squares post-calibration fit. (*a*) Calibration points and corresponding fitted curves. (*b*) Relative difference U_{rel} of the calibrations compared to the combined calibration fit.

To estimate the error from this minimal drift, all data were processed using pre- and post-measurement calibrations separately and values of κ were compared to the values found using combined calibration curves. Despite the agreement apparent in figure 10, regression fit to (1.1) showed differences in κ of up to 1.1 %, whereas fits to (1.3) and (1.4) had variations up to 6.3 % and 5.5 % respectively. Additionally, an interpolation scheme was also attempted to transition between pre- and post-measurement calibration curves over the course of the profile measurements. When this was employed, the estimate of κ from regression fit was found to vary up to 0.6 % and that to (1.3) and (1.4) varied 4.6 % and 4.6 % respectively. Therefore it can be seen that even a slight variation in probe response over the course of a profile measurement will significantly impact the estimate of κ and thus mean velocity measurements with hot wires must be treated with caution.

A.5. *Use of multiple transducers over a large Reynolds-numbers range*

The advantage of the Superpipe is not strictly the high Reynolds numbers it can achieve, but also its achievable Reynolds-number range. It is this range, achieved by pressurizing the working fluid, that makes the use of (1.3) and (1.4) feasible for obtaining estimates of κ. It is also the insensitivity of (1.3) and (1.4) to the bias errors discussed in §§A.1–A.3 that makes them attractive for estimating κ. However, measuring the quantities in (1.3) and (1.4) accurately over the range of Superpipe operating pressures requires the use of multiple pressure transducers of varying sensitivity, each of which requires individual calibration. Therefore, the final source of bias error that will be described here is the error associated with using multiple transducers to measure the quantities used in (1.3) and (1.4). This error will arise from even slight differences in the calibrations between the different transducers.

To illustrate the impact that this error could have on the estimate of κ, we re-analysed the MV data set after artificially adding a -1 % error in the Pitot transducer for $2.5 \times 10^5 \leqslant Re_D \leqslant 1 \times 10^6$ and 1 % error for $Re_D \geqslant 6 \times 10^6$. Whereas

κ determined by (1.1) changed by 0.5 % and −0.5 % respectively in the affected Reynolds-number ranges, κ determined from (1.3) and (1.4) were found to change by −1.5 % to −8 %, depending on the Reynolds-number range used for the fit. A similar analysis conducted with the bias applied to the pressure gradient transducer resulted in a 1–8 % change in κ using (1.3) and (1.4) and −0.5 % and +0.5 % using (1.1). Estimates of κ were found to be much less sensitive to bias errors in the transducer used to measure the Superpipe operating pressure, with a negligible effect on estimates using (1.1) and only a 0.1–0.5 % bias resulting when using (1.3) and (1.4).

Appendix B. Overview of uncertainty estimation process

One of the primary goals of this study was to provide a detailed estimate of the accuracy to which we can experimentally determine κ. To do this, we employed a Monte Carlo-based error analysis, so that variables such as integration scheme and number of data points used in the regression fits would also be factored into the final uncertainty estimate. Here we describe the approach used.

We start by first identifying the directly measured quantities that lead to the estimate of κ. These are: the pressure gradient along the pipe, $\mathrm{d}P/\mathrm{d}x$; the tunnel temperature, T; the tunnel pressure, P; the distance from the wall, y; the pipe radius, R; for Pitot probes, the difference between total and static pressure, ΔP; and for hot-wire probes, to simplify the analysis, we start with the mean hot-wire velocity U after applying the calibration constants. Each measured quantity, ϕ_m, was then assumed to differ from the true quantity, ϕ, by both precision and bias errors such that $\phi_m = \phi(1 + p + b)$, where p and b are the precision and bias errors expressed as a percentage of ϕ.

The errors in derived quantities, u_τ, and viscous length, δ_ν, are then

$$(u_\tau)_m = u_\tau \frac{(1 + p_{\mathrm{d}P/\mathrm{d}x} + b_{\mathrm{d}P/\mathrm{d}x})^{0.5}(1 + b_R)^{0.5}(1 + p_T + b_T)^{0.5}}{(1 + p_P + b_P)^{0.5}}, \tag{B 1}$$

$$(\delta_\nu)_m = \delta_\nu \frac{(1 + p_\mu + b_\mu)(1 + p_T + b_T)^{0.5}}{(1 + p_{\mathrm{d}P/\mathrm{d}x} + b_{\mathrm{d}P/\mathrm{d}x})^{0.5}(1 + b_R)^{0.5}(1 + p_P + b_P)^{0.5}}, \tag{B 2}$$

where, since it was only measured once, the error in pipe radius is treated as a bias error. Similarly, for the Pitot probe measurements

$$U_m = U \frac{(1 + p_{\Delta P} + b_{\Delta P})^{0.5}(1 + p_T + b_T)^{0.5}(1 + b_{corr} + p_{corr})}{(1 + p_P + b_P)^{0.5}}, \tag{B 3}$$

where b_{corr} and p_{corr} represent the bias and precision error introduced by the corrections. For the hot-wire probes we use

$$U_m = U \frac{(1 + p_{\Delta P} + b_{\Delta P})^{0.5}(1 + p_T + b_T)^{0.5}}{(1 + p_P + b_P)^{0.5}(1 + b_{fit})(1 + b_{drift})(1 + p_U)}, \tag{B 4}$$

where the first three error terms are introduced by the Pitot probe used during calibration and b_{fit} and b_{drift} are the errors associated with calibration curve fitting and anemometer drift (here both are assumed to be approximately 1 %). As these terms are all bias errors, an additional term p_U is introduced to account for the precision uncertainty.

We then assume that the value measured during the experiment is the true value, and perturb this value by precision and bias errors estimated using a Gaussian random

number generator and then determine the value of κ using (1.1), (1.3) and (1.4). This process is repeated for 10 000 iterations and the resulting spread in κ estimates used to quantify the uncertainty in the estimated value. The procedure was found to be insensitive to the number of iterations by comparison to runs of 1000 and 10 000 iterations.

For each run, care is taken to ensure that precision and bias errors are properly applied. For example, a separate random number is used for $p_{\Delta P}$ in each Pitot profile, but, following the discussion in § A.5, $b_{\Delta P}$ is kept constant for the range of Reynolds numbers in which the same transducer is used. Error magnitude is estimated using the values cited in table 1 as the 95 % confidence limits.

REFERENCES

BAILEY, S. C. C., HULTMARK, M., MONTY, J. P., ALFREDSSON, P. H., CHONG, M. S., DUNCAN, R. D., FRANSSON, J. H. M., HUTCHINS, N., MARUSIC, I., MCKEON, B. J., NAGIB, H. M., ÖRLÜ, R., SEGALINI, A., SMITS, A. J. & VINUESA, R. 2013 Obtaining accurate mean velocity measurements in high Reynolds number turbulent boundary layers using Pitot tubes. *J. Fluid Mech.* **715**, 642–670.

BAILEY, S. C. C., KUNKEL, G. J., HULTMARK, M., VALLIKIVI, M., HILL, J. P., MEYER, K. A., TSAY, C., ARNOLD, C. B. & SMITS, A. J. 2010 Turbulence measurements using a nanoscale thermal anemometry probe. *J. Fluid Mech.* **663**, 160–179.

BRADSHAW, P. & HUANG, G. P. 1995 The law of the wall in turbulent flow. *Proc. R. Soc. Lond.* A **451**, 165–188.

BUSCHMANN, M. & GAD-EL HAK, M. 2007 Recent developments in scaling of wall-bounded flows. *Prog. Aerosp. Sci.* **42**, 419–467.

COLES, D. E. 1956 The law of the wake in the turbulent boundary layer. *J. Fluid Mech.* **1**, 191–226.

COLES, D. E. & HIRST, E. A. 1968 The young person's guide to the data. In *Proceedings of Computation of Turbulent Boundary Layers*, Vol. II, AFOSR-IFP-Stanford Conference.

GEORGE, W. K. 2007 Is there a universal log law for turbulent wall-bounded flows? *Phil. Trans. R. Soc. Lond.* A **365**, 789–806.

GEORGE, W. K. & CASTILLO, L. 1997 Zero-pressure-gradient turbulent boundary layer. *Appl. Mech. Rev.* **50**, 689–729.

HUFFMAN, G. D. & BRADSHAW, P. 1972 A note on von Kármán's constant in low Reynolds number turbulent flows. *J. Fluid Mech.* **53**, 45–60.

HULTMARK, M., BAILEY, S. C. C. & SMITS, A. J. 2010 Scaling of near-wall turbulence in pipe flow. *J. Fluid Mech.* **649**, 103–113.

HULTMARK, M., VALLIKIVI, M., BAILEY, S. C. C. & SMITS, A. J. 2012 Turbulent pipe flow at extreme Reynolds numbers. *Phys. Rev. Lett.* **108** (9), 094501.

HULTMARK, M., VALLIKIVI, M., BAILEY, S. C. C. & SMITS, A. J. 2013 Logarithmic scaling of turbulence in smooth- and rough-wall pipe flow. *J. Fluid Mech.* **728**, 376–395.

HUTCHINS, N. & CHOI, K.-S. 2002 Accurate measurements of local skin friction coefficient using hot-wire anemometry. *Prog. Aerosp. Sci.* **38** (45), 421–446.

JIMÉNEZ, J. & MOSER, R. D. 2007 What are we learning from simulating wall turbulence? *Phil. Trans. R. Soc. Lond.* A **365**, 715–732.

VON KÁRMÁN, T. 1930 Mechanische Ähnlichkeit und Turbulenz. In *Proceedings of the 3rd International Congress on Applied Mechanics*.

KLEWICKI, J. C., FIFE, P. & WEI, T. 2009 On the logarithmic mean profile. *J. Fluid Mech.* **638**, 73–93.

MARUSIC, I., MCKEON, B. J., MONKEWITZ, P. A., NAGIB, H. M., SMITS, A. J. & SREENIVASAN, K. R. 2010 Wall-bounded turbulent flows: recent advances and key issues. *Phys. Fluids* **22**, 065103.

MARUSIC, I., MONTY, J. P., HULTMARK, M. & SMITS, A. J. 2013 On the logarithmic region in wall turbulence. *J. Fluid Mech.* **716**, R3.

McKeon, B. J. 2003 High Reynolds number turbulent pipe flow. PhD thesis, Princeton University.

McKeon, B. J., Li, J., Jiang, W., Morrison, J. F. & Smits, A. J. 2003 Pitot probe corrections in fully developed turbulent pipe flow. *Meas. Sci. Technol.* **14** (8), 1449–1458.

McKeon, B. J., Li, J., Jiang, W., Morrison, J. F. & Smits, A. J. 2004*a* Further observations on the mean velocity distribution in fully developed pipe flow. *J. Fluid Mech.* **501**, 135–147.

McKeon, B. J. & Smits, A. J. 2002 Static pressure correction in high Reynolds number fully developed turbulent pipe flow. *Meas. Sci. Technol.* **13**, 1608–1614.

McKeon, B. J., Swanson, C. J., Zagarola, M. V., Donnelly, R. J. & Smits, A. J. 2004*b* Friction factors for smooth pipe flow. *J. Fluid Mech.* **511**, 41–44.

Millikan, C. B. 1938 A critical discussion of turbulent flows in channels and circular tubes. In *Proceedings of the Fifth International Congress of Applied Mechanics, Cambridge, MA*.

Monty, J. P. 2005 Developments in smooth wall turbulent duct flows. PhD thesis, University of Melbourne.

Morrison, J. F., McKeon, B. J., Jiang, W. & Smits, A. J. 2004 Scaling of the streamwise velocity component in turbulent pipe flow. *J. Fluid Mech.* **508**, 99–131.

Nagib, H. M. & Chauhan, K. A. 2008 Variations of von Kármán coefficient in canonical flows. *Phys. Fluids* **20**, 101518.

Örlü, R., Fransson, J. H. M. & Alfredsson, P. H. 2010 On near wall measurements of wall bounded flows – the necessity of an accurate determination of the wall position. *Prog. Aerosp. Sci.* **46**, 353–387.

Österlund, J. M., Johansson, A. V., Nagib, H. M. & Hites, M. H. 2000 A note on the overlap region in turbulent boundary layers. *Phys. Fluids* **12** (1), 1–4.

Perry, A. E., Hafez, S. & Chong, M. S. 2001 A possible reinterpretation of the Princeton Superpipe data. *J. Fluid Mech.* **439**, 395–401.

Prandtl, L. 1925 Bericht über Untersuchungen zur ausgebildeten Turbulenz. *Z. Angew. Math. Mech.* **5** (2), 136–139.

Schlichting, H. & Gersten, K. 2000 *Boundary Layer Theory*. 8th edn Springer.

Schultz, M. P. & Flack, K. A. 2013 Reynolds-number scaling of turbulent channel flow. *Phys. Fluids* **25**, 025104.

Smits, A. J., McKeon, B. J. & Marusic, I. 2011 High Reynolds number wall turbulence. *Annu. Rev. Fluid Mech.* **43**, 353–375.

Swanson, C. J., Julian, B., Ihas, G. G. & Donnelly, R. J. 2002 Pipe flow measurements over a wide range of Reynolds numbers using liquid helium and various gases. *J. Fluid Mech.* **461**, 51–60.

Tavoularis, S. 2005 *Measurement in Fluid Mechanics*. Cambridge University Press.

Tropea, C., Yarin, A. & Foss, J. (Eds) 2007 *Springer Handbook of Experimental Fluid Mechanics*. Springer.

Vallikivi, M. 2014 Wall-bounded turbulence at high Reynolds numbers. PhD thesis, Princeton University.

Vallikivi, M. & Smits, A. J. 2014 Fabrication and characterization of a novel nanoscale thermal anemometry probe. *J. MEMS* **99**, doi:10.1109/JMEMS.2014.2299276.

Zagarola, M. V. 1996 Mean-flow scaling of turbulent pipe flow. PhD thesis, Princeton University.

Zagarola, M. V. & Smits, A. J. 1998 Mean-flow scaling of turbulent pipe flow. *J. Fluid Mech.* **373**, 33–79.

Zanoun, E.-S., Durst, F. & Nagib, H. 2003 Evaluating the law of the wall in two-dimensional fully developed turbulent channel flows. *Phys. Fluids* **15** (10), 3079–3089.